Hindawi
Geofluids
Volume 2022, Article ID 8038085, 16 pages
https://doi.org/10.1155/2022/8038085

Research Article

Investigation of the Hydraulic Fracture Propagation Law of Layered Rock Strata Using the Discrete-Particle Model

Xin Zhang [1] and Mei Yin [2]

[1]Department of Mining Engineering, Shanxi Institute of Energy, China
[2]Department of Civil and Environmental Engineering, College of Engineering, Brunel University, UK

Correspondence should be addressed to Xin Zhang; tyzyqhzx@163.com and Mei Yin; mei.yin@brunel.ac.uk

Received 26 January 2022; Accepted 22 March 2022; Published 26 April 2022

Academic Editor: Zhongguang Sun

Hydraulic fracturing is a rock structure transformation method that significantly weakens the mechanical properties of the hard roof strata. Considering the poor hydraulic fracturing effect of special structure such as composite layered rock, this paper carries out hydraulic fracturing numerical simulation experiments and compares the hydraulic fracture morphology and bedding plane interaction mode under different injection rate and injection modes. The experimental results show that the bedding plane can change the trajectory and propagation direction of hydraulic fracture. Under the low injection rate, hydraulic fracturing is conducive to open the bedding plane, but the expansion length of the main hydraulic fracture is easy to be limited. Under the high injection rate, the hydraulic fracture can extend for a long distance. But the fracture morphology tends to be slender and single, which is not conducive to the formation of fracture network. Compared with conventional hydraulic fracturing, stepped variable injection rate hydraulic fracturing can activate more bedding planes, so as to improve the effect of rock strata transformation. The experimental results are instructive in achieving effective control of composite layered rock.

1. Introduction

Hard roof strata refer to the large area of hard rock above the coal. In the process of coal excavation, if the hard roof strata cannot collapse in time, it is very easy to form a large area of suspended roof [1] and induce dynamic disasters [2–4]. Therefore, in the actual production process, it is usually necessary to weaken the hard roof strata with the help of manual means [5, 6]. Hydraulic fracturing technology can change rock internal structure [7, 8], make the roof strata fall fully and timely, and realize the weakening of surrounding rock and stress transfer. It is the key technical approach to weaken the hard roof strata of coal seam [9–12].

Hydraulic fracturing technology was successfully applied in Kansas for the first time in 1947 [13, 14]. After more than 70 years of development, hydraulic fracturing has achieved fruitful results from theory to application [15–17]. By injecting fracturing fluid into closed boreholes, the high water pressure would change the stress state of rocks around boreholes. As a result, a large number of main hydraulic fractures and secondary fractures in rock would be produced, which causes hole wall cracking and artificially transforms the internal structure of rock mass. Compared with the traditional blasting roof weakening technology, hydraulic fracturing has the advantages of simple operation, less quantities, long control distance, and low economic cost [18–20]. Therefore, hydraulic fracturing technology has more advantages in deep rock formation reconstruction.

The fracture morphology is the focus of attention of hydrofracturing construction design [21–23]. Relevant experiments and theories show that the hydraulic fracture in the complete rock matrix is usually perpendicular to the minimum in situ stress [24–27]. Under the influence of long-term geological structure and sedimentation, the upper roof strata have obvious layered characteristics, that is, one or more groups of dominant bedding planes are distributed between rocks [28, 29]. Compared with homogeneous rock, the structural components of composite layered rock are relatively complex and show strong heterogeneity. Therefore, the propagation path of fracture in composite layered rock

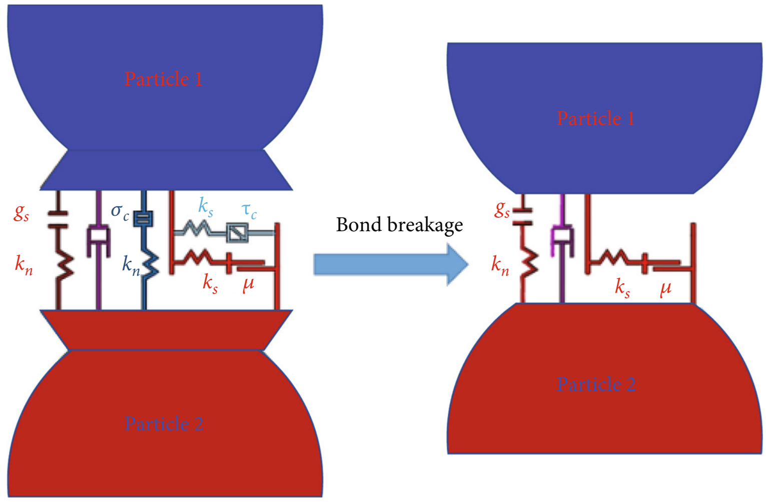

Figure 1: Parallel bond model in PFC^{2D}: (a) parallel bond; (b) bond failure.

is significantly different from that in homogeneous rock [30–32]. For composite layered rock strata, the control effect of bedding plane structure on hydraulic fracture morphology should be emphatically analyzed.

In layered rock strata, the hydraulic fracture morphology has unique characteristics and complexity [33–37]. Previous hydrofracturing experiments generally install a group of artificial fractures in the poured homogeneous test block to study the influence of weak surface. The research shows that hydraulic fracture appears penetration, steering, capture, and bifurcation at the weak surface under the action of original rock stress, mechanical properties of weak surface, and intersection angle [23, 38, 39]. The above research provides good references, but there are also some limitations. In previous studies, most of them focus on small-scale artificial fractures with obvious gap between the extension length of structural plane and rock stratum, which cannot fully reflect the fracture propagation under the large-scale plane [40–42].

The previous experimental research on hydraulic fracturing mainly focuses on geological factors such as principal stress and bedding mechanical properties [43–46]. The geological factors are the original occurrence state of rock, which is difficult to change in actual construction [47, 48]. Therefore, the guiding significance of on-site hydraulic fracturing construction is relatively limited. At present, there are few research works on the hydrofracturing of layered rock under the influence of different operation factors. In addition, relevant field cases show that the hydraulic fracture length is often less than the predicted value, and the actual transformation scale is small when hydraulic fracturing is carried out on this kind of composite layered rock. At present, there is no reasonable explanation for this situation.

Considering the difficulty of collecting composite layered rock test blocks in coal mine working face and the vulnerability of the original occurrence state of the test block in the process of transportation and processing, it is difficult to study the hydrofracturing of composite layered rock under laboratory conditions. The numerical simulation is an effective method to study this problem [49–51]. The basic idea of discrete element method (DEM) is to treat rock materials as a collection of rigid elements separated from discontinuous bodies [52, 53] so that each rigid element can meet the motion equation. The macroscopic mechanical manifestations such as stress, strain, and deformation in the interior of the rock material under external loading can be obtained directly based on the discrete unit method. At the same time, micromechanical information such as movement, arrangement, and contact force changes of the particles can be recorded to establish the connection between macroscopic and micromechanical characteristics. The discrete unit method takes full account of the discontinuous and discrete characteristics of rock materials and thus has significant advantages in modeling problems associated with hydraulic fracturing of composite layered strata [54, 55].

To sum up, this paper takes the composite layered rock as the research object. The particle flow code (PFC^{2D}) is adopted to carry out hydrofracturing experiment under different operating factors (injection rate and injection mode). The fracture morphology of the layered rock is studied. The construction conditions for the best reconstruction effect of composite layered rock are discussed. The research results have some reference value to improve the hydraulic fracturing reconstruction effect, optimize the field construction technology, and effectively predict the hydraulic fracture.

2. Particle Flow Code Contact Model

2.1. Parallel Bond Model (BPM). The parallel bond model in the particle flow code describes the rock behaviors in the way of cemented granular materials [52, 53]. The bonding material can be regarded as two groups of springs on the surface of the sphere (Figure 1), which can transmit stress and torque. If tangential or normal contact force between particles is greater than ultimate strength, the bond between particles will be destroyed, the contact will disappear, and microcracks will be formed at the contact connection. The

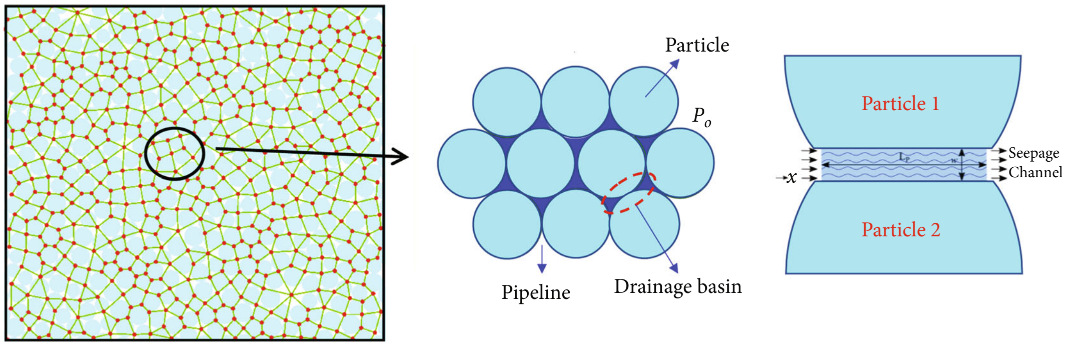

Figure 2: Fluid-solid coupling model in PFC^{2D}.

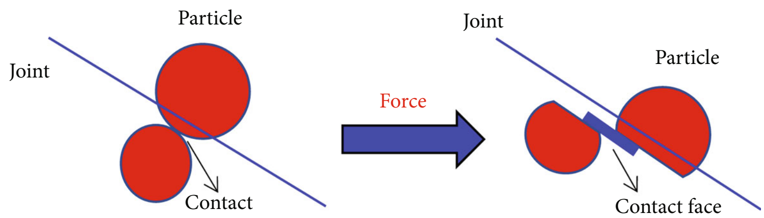

Figure 3: Smooth joint model in PFC^{2D}.

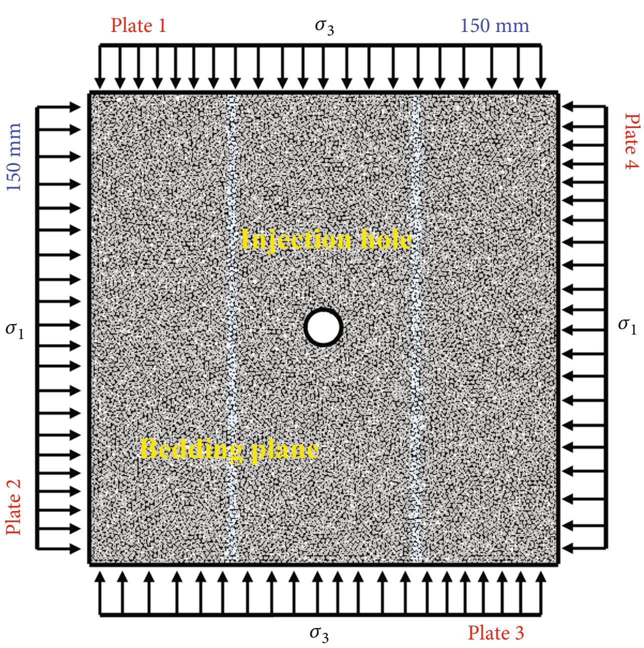

Figure 4: Numerical simulation sample of composite layered rock.

microcracks will expand and fuse with each other to form macrocracks [51, 56–58].

2.2. Fluid-Solid Coupling Model. The fluid-solid coupling algorithm in particle flow code assumes that the contact is the flow path (pipe). The closed polygon area of multiple pipe sieges is a domain. The domain is a unit for storing pressure. The channels between domains can realize the free flow of fluid in the domain (Figure 2). The seepage path of fluid is generalized as a parallel plate channel. The real-time updated fluid pressure acts on different particles, causing the change of domain volume, thus changing the contact force and the width of fluid pipeline. When the bearing limit of particles is overcome, hydraulic fractures are formed.

2.3. Smooth Joint Model (SJM). The smooth joint model allows the particles to overlap and slide along the bedding plane, avoiding the normal movement of particles along the contact surface, so as to more truly simulate the work transport characteristics of bedding particles (Figure 3). Based on the particle flow code, all mesoparameters (except dip and dip) of the smooth joint model can be equivalent transformed with BPM mesoparameters, and the normal strength and cohesion of the smooth joint model are not zero. In addition, the smooth joint model meets the Coulomb criterion, and the tangential strength (τ_c) of the joint is determined by cohesion $(\bar{c}_b)$, internal friction angle $(\bar{\Phi}_b)$, and normal stress (σ) acting on the joint surface:

$$\tau_c = \bar{c}_b + \sigma \tan \bar{\Phi}_b. \quad (1)$$

If the maximum shear stress (F_s) is greater than the tangential strength, the joint bond will undergo shear failure.

3. Modeling Approach and Experimental Scheme

3.1. Modeling Approach. The composite layered rock simulation block is shown in Figure 4. The size of the square block is 150 mm × 150 mm, consisting of three rock substrates and two bedding planes. The color of the rock matrix is set to gray, and the color of the bedding planes is arranged as light

Table 1: Mechanical parameters of each part of the test block.

Uniaxial compressive strength σ_c (MPa)	Modulus of elasticity E (GPa)	Tensile strength σ_t (MPa)	Bedding tensile strength σ_t (MPa)	Cohesion c (MPa)	Bedding cohesion c (MPa)	Angle of internal friction φ (°)	Fracture toughness K_{1c} ($N \cdot mm^{3/2}$)
15.85	24.75	4.07	0.39	27.38	2.13	18.97	13.23

Table 2: Sample microscopic parameters.

Particle parameters					Parallel bonding parameters				
E_c (GPa)	k_n/k_s	μ	R_{max}/R_{max}	ρ	$\bar{E}_c$ (GPa)	$\bar{k}_n/\bar{k}_s$	$\bar{\sigma}_c$ (MPa)	$\bar{c}$ (MPa)	$\bar{\lambda}$
1.63	1	0.1	1.54	2.65	1.63	1	5.9	16.2	1

Table 3: Experimental scheme.

Test name	Confining pressure (MPa)			The injection mode	Bedding plane cementation strength (MPa)	The injection rate of fracturing fluid (ml/min)
	σ_1	σ_2	σ_3			
Laboratory test	6	4.5	3	Conventional fracturing	0.39	200
Simulated test	6		3	Conventional fracturing	0.39	200

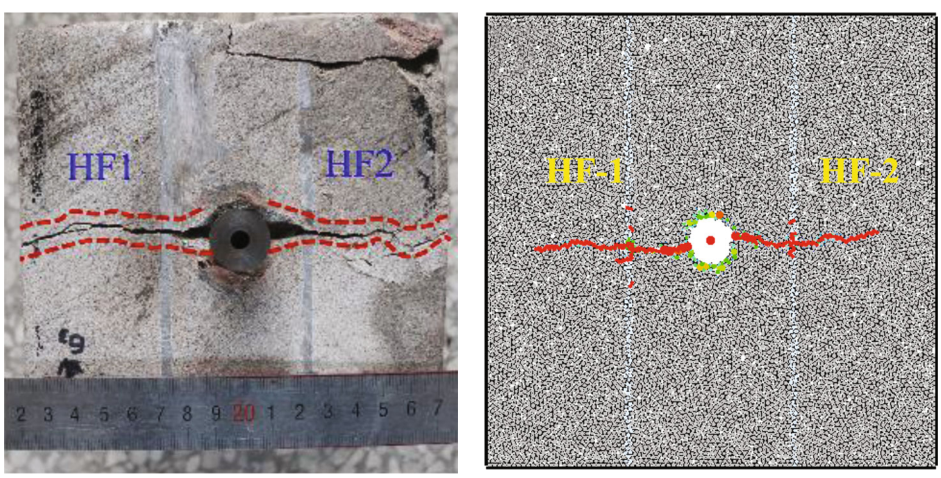

(a) (b)

Figure 5: Hydraulic fracture morphology: (a) laboratory test; (b) simulated test.

Table 4: Experimental scheme for hydrofracturing under different injection rates.

Test name	Confining pressure (MPa)		The injection mode	Bedding plane cementation strength (MPa)	The injection rate of fracturing fluid (ml/min)
	σ_1	σ_3			
1-1	6	3	Conventional fracturing	0.39	200
1-2	6	3	Conventional fracturing	0.39	100
1-3	6	3	Conventional fracturing	0.39	50

blue. Excavate a borehole at the center of the sample, the thickness data of single bedding plane is 3 mm, and loading plates are set around the model. The basic mechanical parameters are given in Table 1. The setting of micromechanical parameters of numerical model refers to the paper of Zhang et al. [59] (Table 2).

Table 5: Experimental scheme for hydrofracturing under different injection modes.

Test name	Confining pressure (MPa) σ_1	Confining pressure (MPa) σ_3	The injection mode	Bedding plane cementation strength (MPa)	The injection rate of fracturing fluid (ml/min)
2-1	6	3	Conventional fracturing	0.39	75
2-2	6	3	Variable fracturing	0.39	40 ⟶ 50 ⟶ 60 ⟶ 70 ⟶ 80 ⟶ 90 ⟶ 100

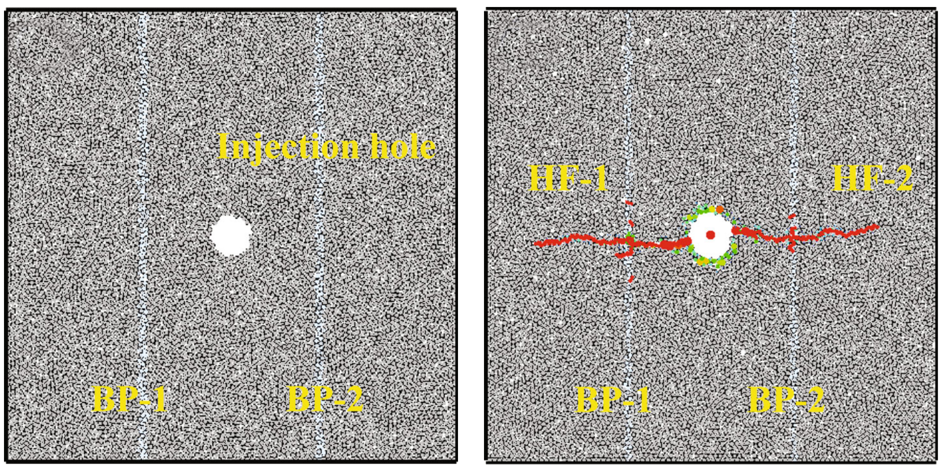

(a) (b)

Figure 6: Group 1-1 hydraulic fracture test: (a) test block before hydraulic fracturing; (b) test block after hydraulic fracturing.

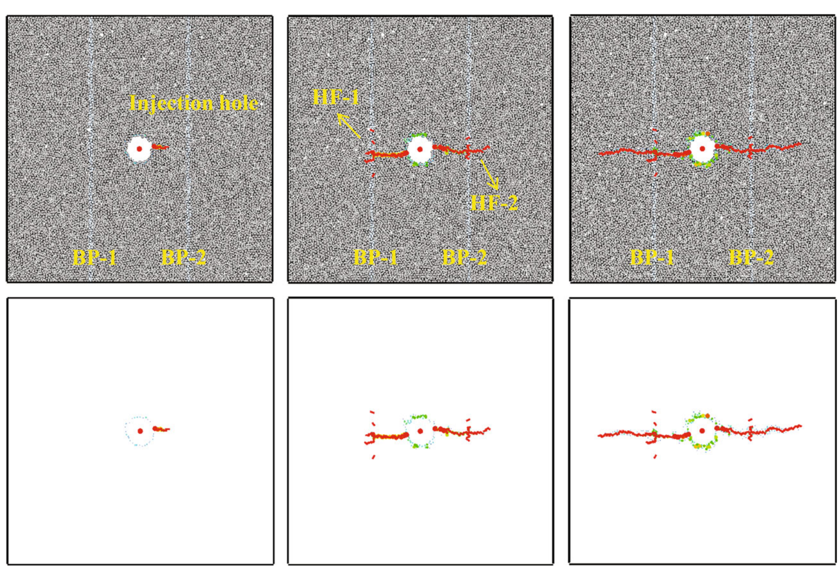

Figure 7: Group 1-1 hydraulic fracture morphology and interactive penetration mode.

3.2. Validity Analysis and Verification of Numerical Model. After the establishment of the numerical model, its effectiveness needs to be analyzed and verified. Referring to the experimental scheme set in the paper of Zhang et al. [39] (Table 3), the hydraulic fracturing experiment is carried out on the simulated sample. The test result is shown in Figure 5. In the numerical model, the hydraulic fracture is perpendicular to stress σ_3. Two hydraulic fractures pass through the bedding plane. The fracture morphology is consistent with the research results of hydrofracturing in the

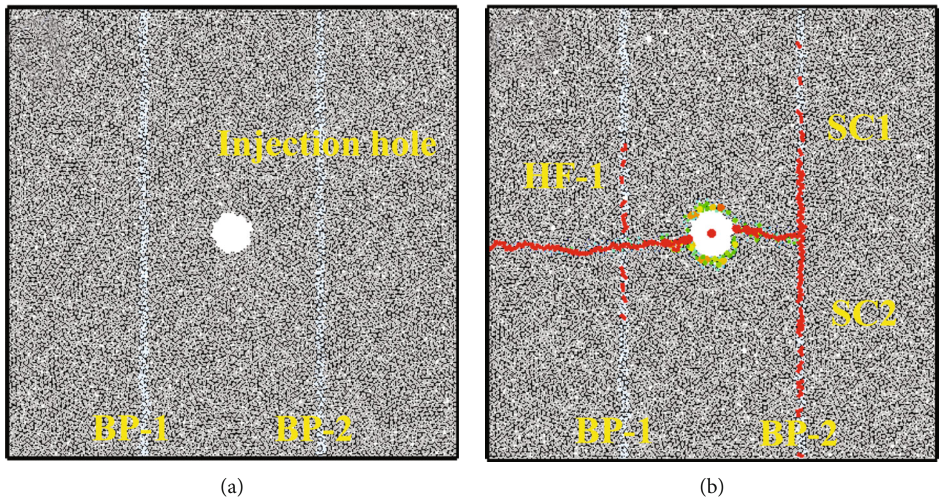

Figure 8: Group 1-2 hydraulic fracture test: (a) test block before hydraulic fracturing; (b) test block after hydraulic fracturing.

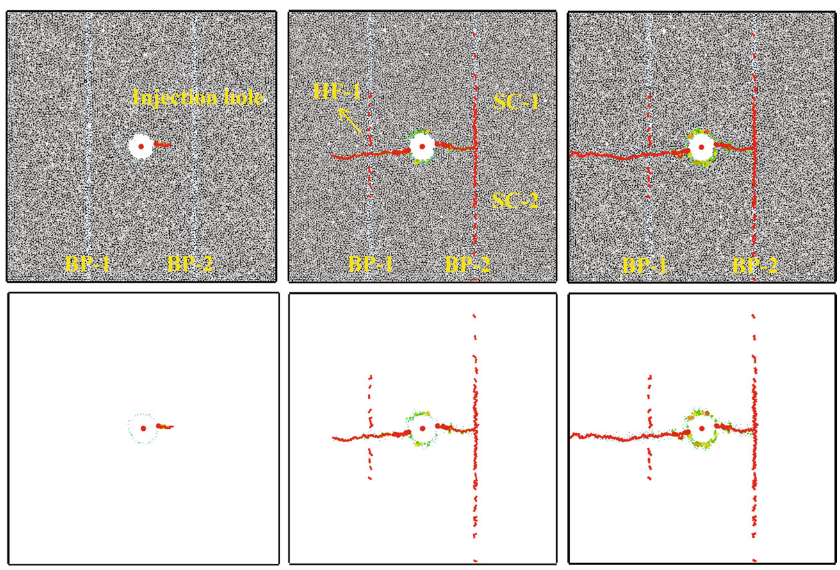

Figure 9: Group 1-2 hydraulic fracture morphology and interactive penetration mode.

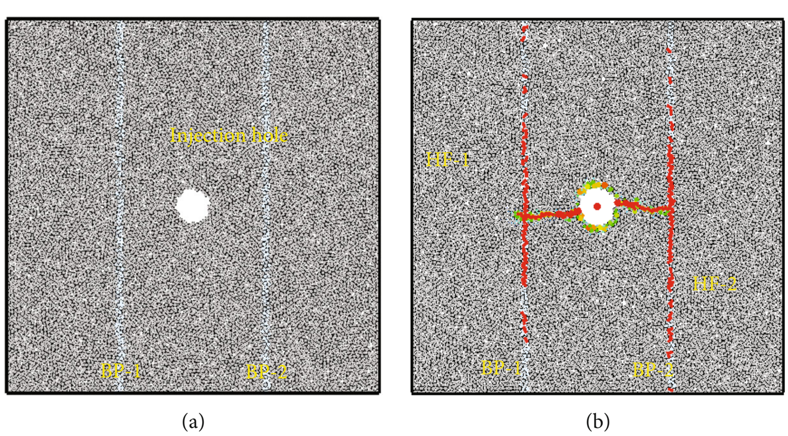

Figure 10: Group 1-3 hydraulic fracture test: (a) test block before hydraulic fracturing; (b) test block after hydraulic fracturing.

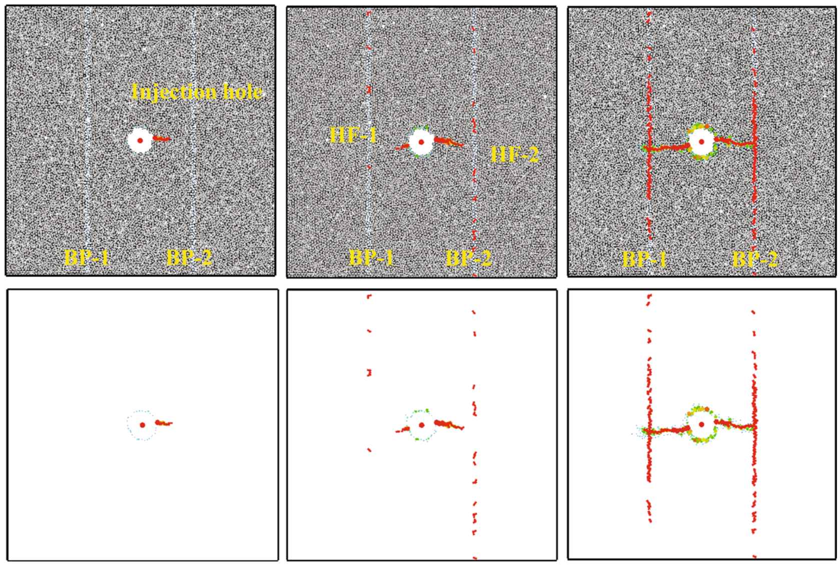

Figure 11: Group 1-3 hydraulic fracture morphology and interactive penetration mode.

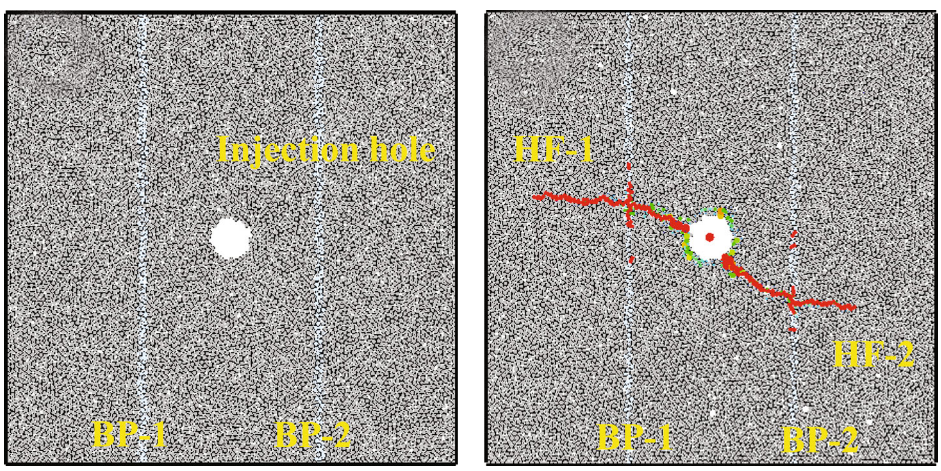

(a) (b)

Figure 12: Group 2-1 hydraulic fracture test: (a) test block before hydraulic fracturing; (b) test block after hydraulic fracturing.

laboratory [60], which fully proves effectiveness of the simulation test. Therefore, hydrofracturing influencing factors of the numerical model can be further analyzed.

4. Hydraulic Fracture Propagation under Different Injection Rates and Injection Modes

4.1. Experimental Scheme. Injection rate and injection mode are the key operating factors to determine the hydraulic fracture morphology. The above two factors will be studied below. For hydraulic fracturing experiments at different injection rates, three groups of different injection rates are set. The hydraulic fracturing experiments at different injection modes are set up two modes, conventional hydraulic fracturing and stepped hydraulic fracturing with increasing fluid rate. The conventional hydraulic fracturing mode is to continuously inject fracturing fluid at a constant injection rate (75 ml/min) until the rock breaks. Stepped variable injection rate hydraulic fracturing mode refers to that the first stage displacement is 40 ml/min, the same injection rate is maintained for 2 minutes, and the injection rate at the next stage is 10 ml/min higher than that of the previous stage. According to this kind of push, continuous injection is carried out between adjacent two stages. The experimental schemes are shown in Tables 4 and 5.

4.2. Hydraulic Fracture Morphology under Different Injection Rates

4.2.1. Group 1-1: The Injection Rate Is 200 ml/min. In order to describe the test results, the left and right wings' hydraulic fractures are named hydraulic fracture-1 (HF1) and hydraulic fracture-2 (HF2). The left and right bedding planes are named bedding plane-1 (BP-1) and bedding

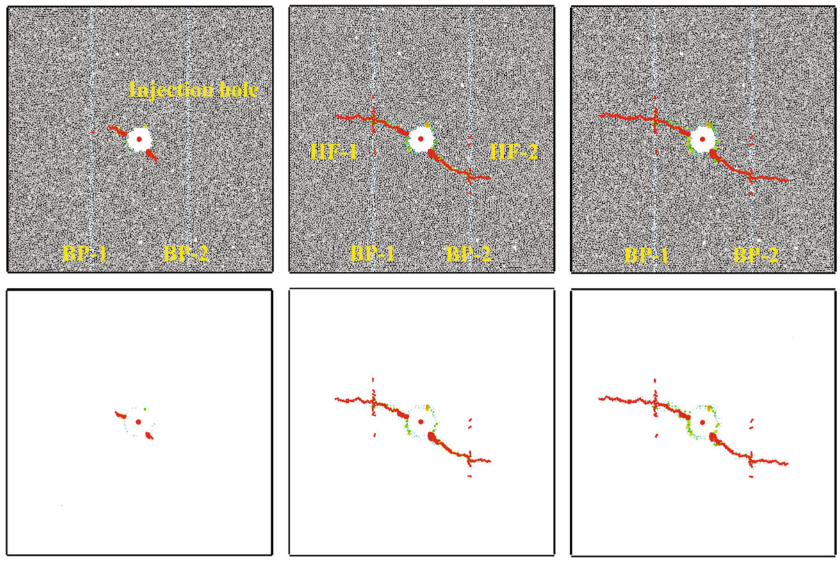

Figure 13: Group 2-1 hydraulic fracture morphology and interactive penetration mode.

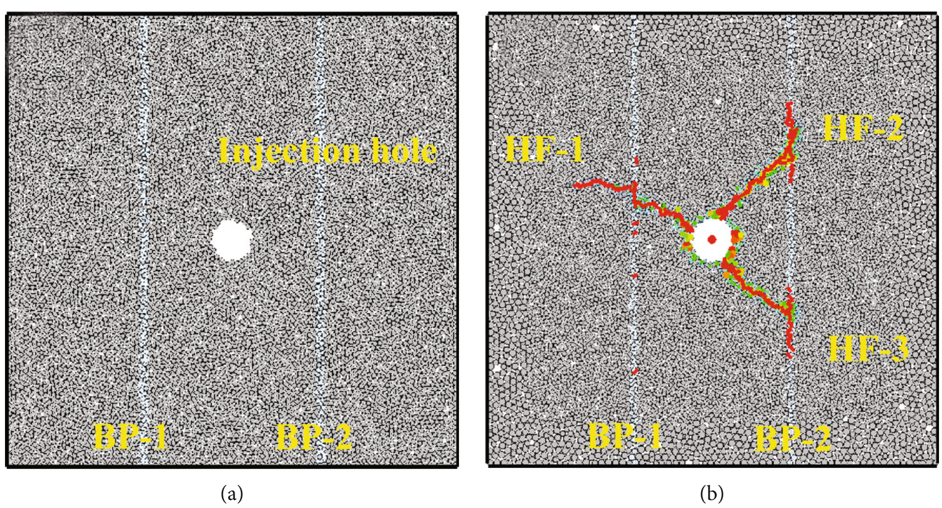

Figure 14: Group 2-2 hydraulic fracture test: (a) test block before hydraulic fracturing; (b) test block after hydraulic fracturing.

plane-2 (BP-2). It can be seen that two main hydraulic fractures are initiated from both sides of the injection hole and propagate along the principal stress σ_1 and finally extend to the test block edge (Figure 6). The hydraulic fractures pass directly through the BP-1 and the BP-2, and the propagation trajectory does not deflect. The hydraulic fracture penetrates the entire test block, dividing the test block into two parts (Figure 7). The overall shape of the hydraulic fractures on the two wings is symmetrically distributed and similar in length.

The fracture trajectory inside the test block is relatively continuous and smooth, and the lines of water pressure front and fracture front are continuous. The overall hydraulic fracture morphology is very similar to the fracture morphology in homogeneous rock, which shows that the hydraulic fracture expansion under the condition of high injection rate is less affected by the bedding plane.

4.2.2. Group 1-2: The Injection Rate Is 100 ml/min. In group 1-2, two main hydraulic fractures initially extend to the BP-1 and BP-2 along the stress σ_1. Then, the left wing fracture maintains the original propagation direction, extends through the BP-1, and finally extends to the Plate-2. The propagation trajectory is continuous without significant deflection (Figure 8).

The right wing main hydraulic fracture (HF2) branches at BP-2. The two branch hydraulic fractures (SC1, SC2) extend along the bedding plane to the Plate-1 and Plate-3 of the test block, respectively. However, the fractures distance extending along the BP-2 is limited, and finally, two branch hydraulic fractures do not extend to the block edge (Figure 9). The reason can be inferred that with the increase of the bedding fracture extension distance, the friction along the way increases gradually. When fracture reaches a certain length, it is difficult to expand without greater driving force.

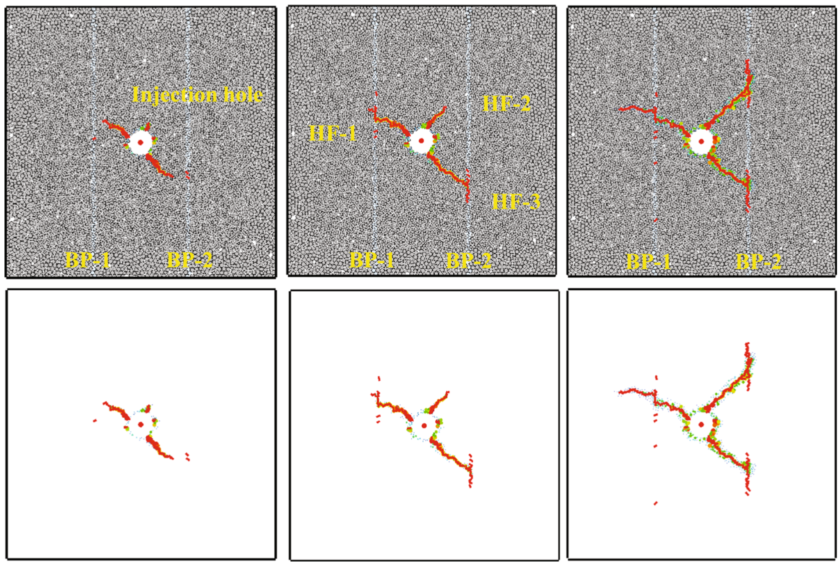

Figure 15: Group 2-2 hydraulic fracture morphology and interactive penetration mode.

In addition, multiple micro fracture concentration areas are formed in BP-1, and a wide range of cracking occurs in BP-2 and the matrix rock mass is almost separated from BP-2.

4.2.3. Group 1-3: The Injection Rate Is 50 ml/min. The two wings' main hydraulic fractures extend to HF1 and HF2 along the stress σ_1. Then, the hydraulic fractures' propagation direction at the bedding planes deflects from σ_1 to σ_3, and the deflection angle reaches 90°. The two wings' hydraulic fractures finally extend to the block edge (Figure 10).

The water pressure front lines are discontinuous. In addition, the bedding planes on two sides showed extensive cracking (Figure 11). The area sandwiched by the two wings' hydraulic fractures forms a separate block, and the matrix rock is completely separated from the bedding planes. Therefore, the range of hydraulic fracturing is limited to the intermediate rock matrix, which shows that bedding has a significant effect on fracture propagation under the low injection rate.

4.3. Morphology of Hydraulic Fracture under Different Injection Modes

4.3.1. Group 2-1: The Conventional Hydraulic Fracturing Mode. There are visible two wings' main hydraulic fractures in the test block (Figure 12). The included angle between the left wing fracture (HF1) direction and the direction of stress σ_1 is 32°. HF1 extends through BP-1; the propagation path does not appear obvious deflection and finally extends to the Plate-2.

The right wing hydraulic fracture (HF2) direction has an included angle of about 53° with the stress σ_1. After the hydraulic fracture expands to BP-2, the propagation path has a slight deflection and finally extends to the Plate-4 (Figure 13). The rock materials in the bedding interaction area are slightly damaged.

4.3.2. Group 2-2: The Stepped Variable Injection Rate Hydraulic Fracturing Mode. Three clear hydraulic fractures appear on the test block, where two hydraulic fractures (HF2, HF3) are distributed on hole right side, and the third hydraulic fracture (HF1) is distributed on the hole left side (Figure 14). The included angle between HF1 and stress σ_1 is about 47°. When hydraulic fracture expands to BP-1, the HF1 expands along the bedding. After extending along bedding for a certain distance, the propagation direction of HF1 changes again and finally HF1 passes through the BP-1 and extends to the middle of the left matrix rock.

The angle between HF2 and stress σ_1 is about 28°. After HF2 extends to BP-2, its spreading direction also changes. HF2 completely expands along BP-2 and finally stops after extending for a certain distance (Figure 15). The angle between the spreading direction of HF3 and stress σ_1 is about 49°. Similar to H2, after HF3 extends to BP-2, HF3 completely expands along BP-2 and stops after extending for a certain distance.

5. Characteristics of Water Pressure Curve and Interactive Modes of Hydraulic Fractures

5.1. Characteristics of Water Pressure Curve under Different Injection Rates. It can be found that the hydrofracturing can be divided into three stages (Figure 16): AB: water pressure accumulation stage; BE: stage of injection hole cracking and continuous expansion of hydraulic fracture; and EF: pump shutdown and pressure relief stage. The burst water pressure (water pressure at initial rupture of borehole wall) of groups 1-1, 1-2, and 1-3 is 15.92, 14.21, and 12.83 MPa. With the increase of injection rate, burst water pressure also increases.

There is a rising section (DE) in the water pressure curve of the stable expansion stage (BE) of three groups, which is significantly different from the homogeneous rock water pressure curve. The reason is that matrix tensile strength is

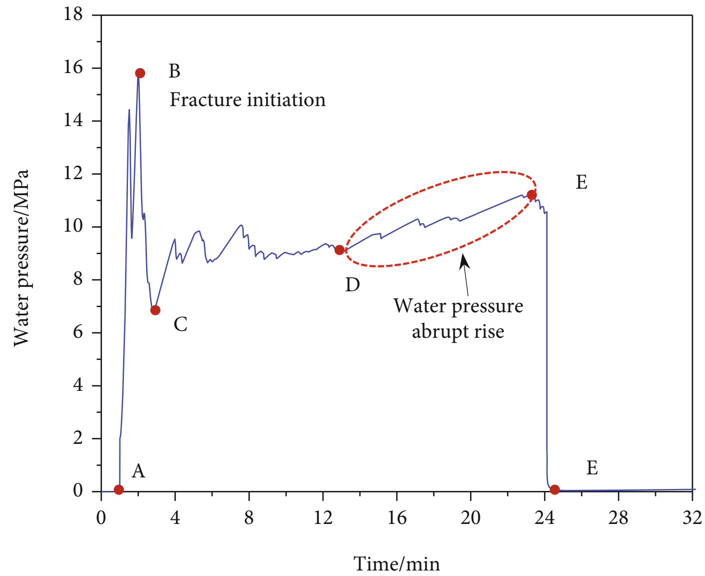

(a) Water pressure curve of group 1-1

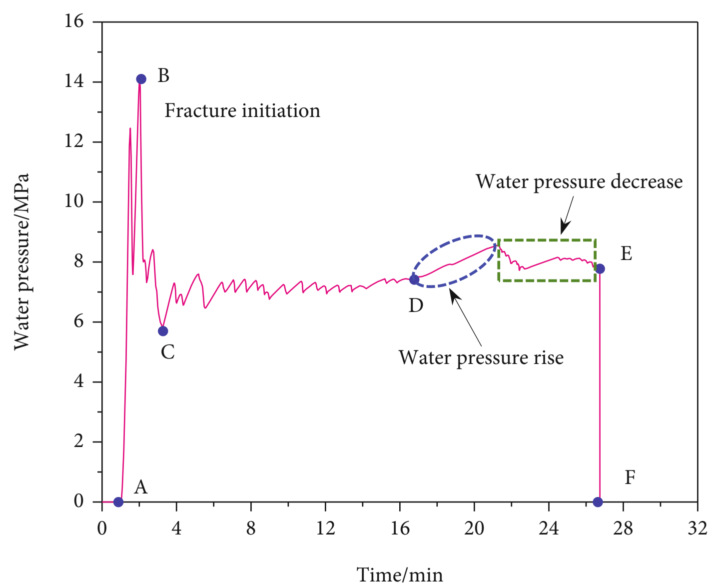

(b) Water pressure curve of group 1-2

FIGURE 16: Continued.

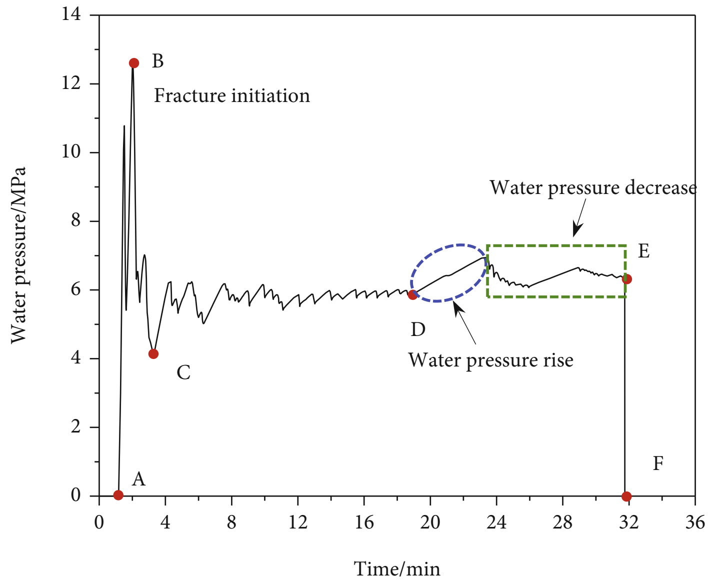

(c) Water pressure curve of group 1-3

Figure 16: Water pressure curve of composite layered rock under different injection rates.

significantly higher than bedding area, and the water pressure required to achieve stable expansion in the rock matrix is high. When the hydraulic fracture extends through the bedding plane into the rock mass, the fracturing fluid needs to accumulate to raise the water pressure. Therefore, there will be a new platform rise stage in the water pressure curve (DE), similar to the initiation stage of hydraulic fracturing.

There is a sudden change in the water pressure curve of the stable expansion stage (BE) of group 1-2 and group 1-3, and the water pressure decreases instantaneously. The reason is that the hydraulic fractures on the right wing of group 1-3 and group 1-2 expand both along the bedding plane. At this time, the resistance of fracture propagation is small and a large amount of fracturing fluid will be dissipated, so the water pressure will decrease rapidly.

5.2. Characteristics of Water Pressure Curve under Different Injection Modes. The burst water pressure of groups 2-1 and 2-2 is 13.84 MPa and 7.58 MPa, respectively (Figure 17). The water pressure curve of the three stages of group 2-1 is similar to that of group 1-1, and there is rising section (DE) in water pressure in the stable expansion stage (BE) of the two groups. The water pressure curve of stepped variable injection rate hydraulic fracturing (group 2-2) is significantly different from that of conventional hydraulic fracturing. Due to the continuous change of injection rate, the water pressure fluctuates periodically between 4 and 11 MPa, reflecting the periodic replacement process of high-pressure fracture opening, pressure relief fracture closing, and pressure rise fracture opening. And the frequency of fracture opening closing is significantly higher than conventional hydrofracturing. Therefore, the water pressure curve of stepped variable injection rate has obvious step characteristics, and the volatility is much higher than conventional hydrofracturing.

When stepped variable injection rate hydrofracturing is adopted, there are many interactive penetration modes. The complexity of water pressure curve is high, which reflects a variety of interactive penetration modes to a certain extent. Therefore, it can be found that the hydraulic fracture interactive penetration mode is obviously consistent with the water pressure curve. Furthermore, it can be found that the peak water pressure in each cycle of group 2-2 shows a fluctuating increase with the increase of the injection rate. This phenomenon further confirms the correctness of the conclusions in Section 4.1.

5.3. Interactive Penetration Modes of Hydraulic Fractures. Based on the test results, four interactive penetration modes are summarized: mode I (Figure 18(a)): hydraulic fracture (HF) passes through the bedding plane (BP) along maximum principal stress, the propagation path basically does not deflect, branch, and bifurcation ("/"); mode II (Figure 18(b)): HF not only extends along the BP but also extends through the bedding plane ("≠"); mode III (Figure 18(c)): HF extends completely along the BP to the edge of the test block ("T"); mode IV (Figure 18(d)): HF first extends along the BP for a certain distance and then extends through the BP ("N").

6. Discussion

6.1. Influence of Different Injection Rates on Hydraulic Fracture. By comparing the fracture morphology under different injection rates, it can be found that in group 1-1, the hydraulic fractures on both wings extend through the layer. The hydraulic fractures in groups 1-2 and 1-3 not only pass through the layer but also propagate along the layer. The bedding plane and rock are almost completely cracked in

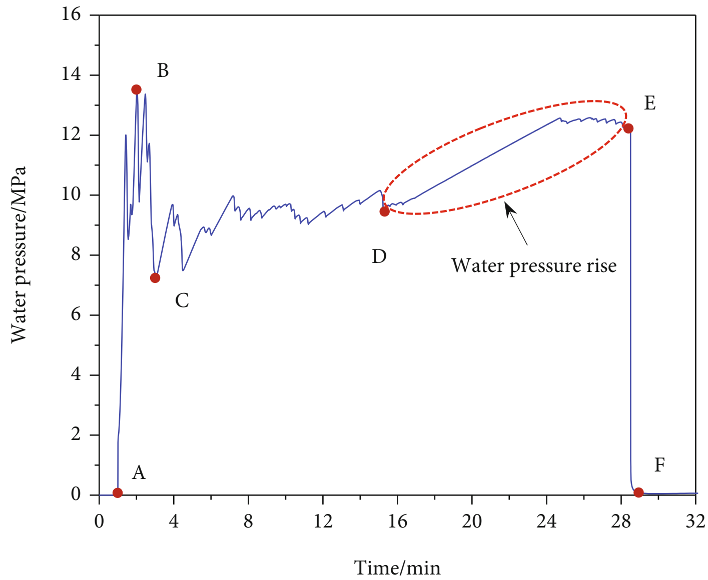

(a) Water pressure curve of group 2-1

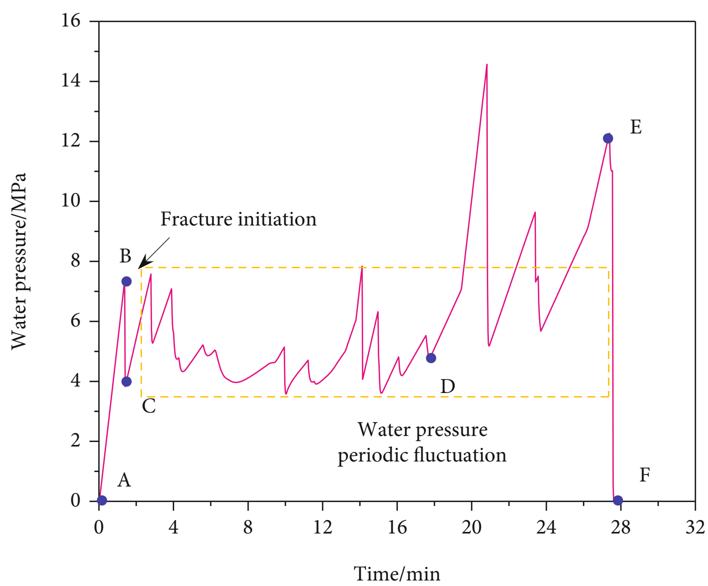

(b) Water pressure curve of group 2-2

Figure 17: Water pressure curve of composite layered rock under different injection modes.

group 1-3, and the bedding opening degree is significantly higher than group 1-2.

The above test results fully show that the injection rate significantly affects the spatial morphology of hydraulic fractures and the interactive penetration mode of bedding plane in composite layered rock. At high liquid injection rate, hydraulic fractures are easier to propagate through bedding plane; at low liquid injection rate, the trapping ability of bedding to hydraulic fractures is stronger. With the increase of liquid injection rate, the interactive penetration mode of hydraulic fractures also changes from extending along bedding plane to passing through the bedding plane.

In view of the hydraulic fracturing construction of on-site composite hard roof, the ideal roof reconstruction effect requires not only the hydraulic fracture to obtain a long enough extension distance but also the good communication between hydraulic fracture and bedding so that the hard roof is collectively “broken.” Based on the above research, if injection rate is set too large, it is difficult to effectively communicate with the bedding plane though the hydraulic fracture has strong penetration ability. The hydraulic fracture is too single and straight, resulting in poor roof reconstruction effect. If injection rate is small, hydraulic fracture is easy to communicate with bedding, but bedding capture effect is too strong, which will lead to the short fracture extension distance, the fracturing range is limited to a certain bedding rock stratum, and the fracture network volume and fracturing range are seriously limited.

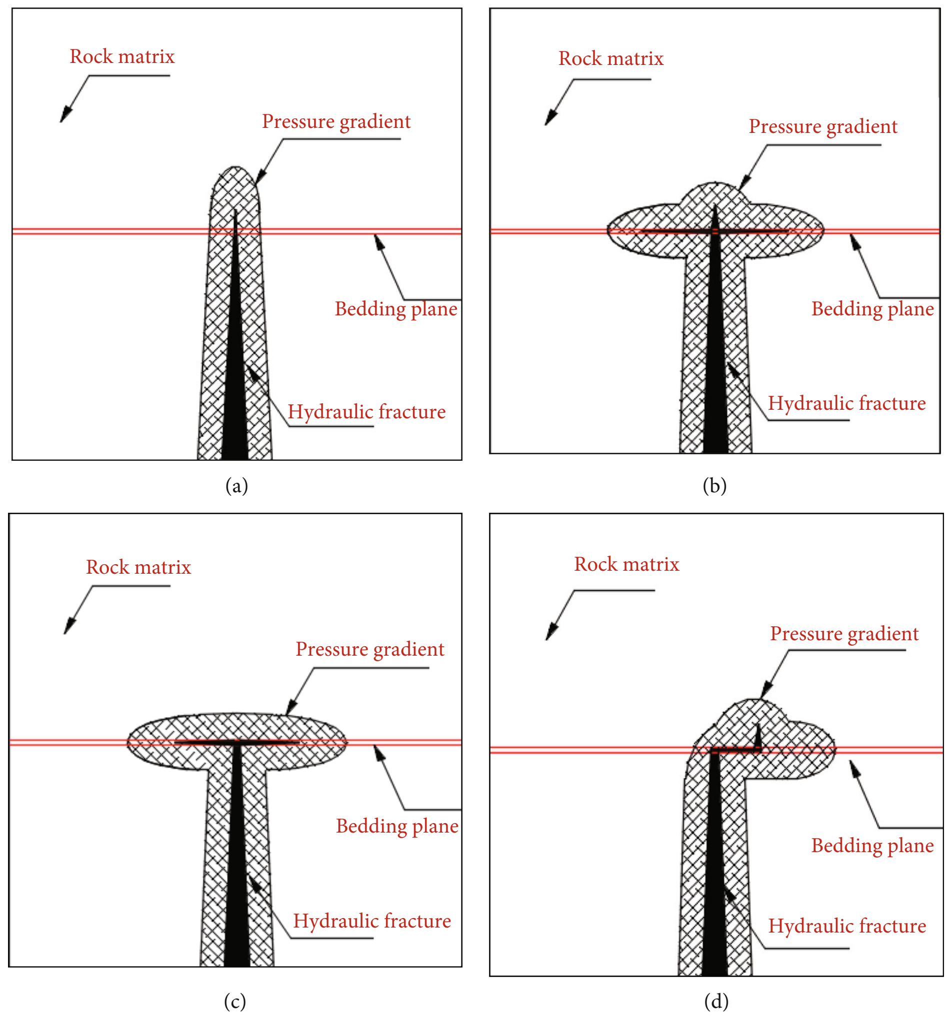

FIGURE 18: Mode of hydraulic fracture extension at bedding plane.

Too large or too small, the fracturing fluid injection rate is not conducive to the structural transformation of hard roof. In general, it is the best to adopt moderate injection rate for composite layered rock.

6.2. Influence of Different Injection Modes on Hydraulic Fracture. It can be seen that the hydraulic fracture propagation patterns under different injection methods are significantly different. Under the conventional hydraulic fracturing mode, slender hydraulic fractures with regular propagation along maximum principal stress are formed in block, and fracture morphology is relatively regular and single. Under the condition of stepped variable injection rate hydraulic fracturing mode, there are many interactive penetration modes, and the fracture propagation path is complex. Compared with conventional hydraulic fracturing, the fracture network volume under stepped variable injection rate hydraulic fracturing is larger and the reconstruction effect is better.

In addition, compared with conventional hydraulic fracturing, stepped variable injection rate hydraulic fracturing can promote the dynamic expansion of hydraulic fractures. Relevant studies have shown that there are two reasons for the formation of dynamic hydraulic fractures [61, 62]: one is the disturbance of rapid loading and unloading behavior caused by hydraulic fracturing to the stability of weak surface. The second is the rapid loading and splitting effect of fluid pressure. When the fracture propagation velocity exceeds a certain threshold, the propagation velocity will be extremely unstable and a dynamic hydraulic fracture will be formed. Fracture bifurcation is an inherent phenomenon in fracture dynamic propagation. Due to the high frequency of fracture opening change, hydraulic fractures are easy to form secondary fractures and bifurcate again in the process of propagation. Based on the above two reasons, the stepped variable injection rate hydraulic fracturing mode can significantly improve the disturbance effect on bedding plane in the process of changing the injection rate and accelerate the fracturing of rock mass at the moment of increasing the injection rate, so as to promote the dynamic expansion of hydraulic fractures.

Therefore, it can be found that under the stepped variable injection rate hydraulic fracturing mode, the hydraulic fracture usually expands for a certain distance along the bedding plane and then changes the expansion direction and passes through the bedding plane, forming a more complex stepped expansion track. The reason is that at the initial stage of variable injection rate hydraulic fracturing, injection rate is low and the water pressure is low. At this time, the hydraulic fracture is easy to expand along the bedding with low required fracture energy. With the injection rate instantaneous increase, the instantaneous liquid injection volume is significantly larger than the expansion volume of hydraulic fracture. At this time, the water pressure at the fracture tip will significantly increase. At the same time, the propagation speed of fracture will fluctuate violently, resulting in dynamic fracture and easy bifurcation. Therefore, when fractures meet weak point and stress concentration point, fracture will turn and expand into rock. Stepped variable injection rate hydraulic fracturing improves the ability of bifurcation fractures and is conducive to the complexity of fracture structure, which will produce more artificial fractures in composite layered rock.

7. Conclusion

(1) The hydrofracturing can be divided into three stages: water pressure accumulation stage, hydraulic fracture continuous expansion stage, and pump shutdown stage. Four different interaction modes can be abstracted. In addition, interactive penetration mode is obviously consistent with the fluctuation state of water pressure curve

(2) If the injection rate is small, the hydraulic fracture is very easy to be captured by the bedding plane, which will seriously limit the fracturing range; if injection rate is too large, hydraulic fracture is difficult to effectively communicate with bedding plane. The effect of adopting a more moderate injection rate for the composite layered rock roof strata is the best

(3) The stepped increase of injection rate will make the hydraulic fracture expand dynamically along multiple fracture points. Compared with conventional hydrofracturing, the fracture extension distance is longer, and more bedding planes can be activated, which is conducive to the formation of complex fracture network

Data Availability

All the data have been included in the manuscript.

Conflicts of Interest

The authors declare no conflict of interest.

Acknowledgments

The authors would like to acknowledge Yuqi Zhang for various contributions that helped to complete this paper.

References

[1] F. Huang, J. Yan, X. Fan et al., "Uncertainty pattern in landslide susceptibility prediction modelling: effects of different landslide boundaries and spatial shape expressions," *Geoscience Frontiers*, vol. 13, no. 2, article 101317, 2022.

[2] X. Hao, W. Du, Y. Zhao et al., "Dynamic tensile behaviour and crack propagation of coal under coupled static- dynamic loading," *International Journal of Mining Science and Technology*, vol. 30, no. 5, pp. 659–668, 2020.

[3] J. Yang, H. Lian, and V. P. Nugyen, "Study of mixed mode I/II cohesive zone models of different rank coals," *Engineering Fracture Mechanics*, vol. 246, article 107611, 2021.

[4] L. You, Y. Kang, Q. Chen, C. Fang, and P. Yang, "Prospect of Shale Gas Recovery Enhancement by Oxidation-Induced Rock Burst," *Natural Gas Industry B*, vol. 4, no. 6, pp. 449–456, 2017.

[5] M. Brook, B. Hebblewhite, and R. Mitra, "Coal mine roof rating (CMRR), rock mass rating (RMR) and strata control: Carborough Downs Mine, Bowen Basin, Australia," *International Journal of Mining Science and Technology*, vol. 30, no. 2, pp. 225–234, 2020.

[6] M. Eremin, G. Esterhuizen, and I. Smolin, "Numerical simulation of roof cavings in several Kuzbass mines using finite- difference continuum damage mechanics approach," *International Journal of Mining Science and Technology*, vol. 30, no. 2, pp. 157–166, 2020.

[7] B. Hebblewhite, "Fracturing, caving propagation and influence of mining on groundwater above longwall panels-a review of predictive models," *International Journal of Mining Science and Technology*, vol. 30, no. 1, pp. 49–54, 2020.

[8] F. Huang, S. Tao, Z. Chang et al., "Efficient and automatic extraction of slope units based on multi-scale segmentation method for landslide assessments," *Landslides*, vol. 18, no. 11, pp. 3715–3731, 2021.

[9] J. Fan, L. Dou, H. Hu et al., "Directional hydraulic fracturing to control hard-roof rockburst in coal mines," *International Journal of Mining Science & Technology*, vol. 22, no. 2, pp. 177–181, 2012.

[10] Z. Guo, Y. Shi, F. Huang, X. Fan, and J. Huang, "Landslide susceptibility zonation method based on C5.0 decision tree and *K*-means cluster algorithms to improve the efficiency of risk management," *Geoscience Frontiers*, vol. 12, no. 6, article 101249, 2021.

[11] Q. He, F. T. Suorineni, and J. Oh, "Review of hydraulic fracturing for preconditioning in cave mining," *Rock Mechanics & Rock Engineering*, vol. 49, no. 12, pp. 4893–4910, 2016.

[12] Z. Zhang, H. Wang, B. Deng, M. Li, and D. Zhang, "Field investigation of hydraulic fracturing in coal seams and its enhancement for methane extraction in the Southeast Sichuan Basin, China," *Energies*, vol. 11, no. 12, p. 3451, 2018.

[13] E. Fjær, R. Holt, P. Horsrud et al., *Petroleum related rock mechanics*, Elsevier, 2008.

[14] M. K. Hubbert and D. G. W. Willis, "Mechanics of hydraulic fracturing," *Transactions of the AIME*, vol. 210, no. 1, pp. 153–168, 1957.

[15] B. Huang, Y. Wang, and S. Cao, "Cavability control by hydraulic fracturing for top coal caving in hard thick coal seams," *International Journal of Rock Mechanics and Mining Sciences*, vol. 74, pp. 45–57, 2015.

[16] Y. Li, Y. Shuai, W. Zhao, W. Li, and J. Zhang, "Experimental of hydraulic fracture propagation using fixed-point multistage

fracturing in a vertical well in tight sandstone reservoir," *Journal of Petroleum Science and Engineering*, vol. 171, pp. 704–713, 2018.

[17] L. C. Murdoch and W. W. Slack, "Forms of hydraulic fractures in shallow fine-grained formations," *Journal of Geotechnical & Geoenvironmental Engineering*, vol. 128, no. 6, pp. 479–487, 2002.

[18] J. Feng, E. Wang, Q. Huang, H. Ding, and X. Zhang, "Experimental and numerical study of failure behavior and mechanism of coal under dynamic compressive loads," *International Journal of Mining Science and Technology*, vol. 30, no. 5, pp. 613–621, 2020.

[19] B. Huang, Q. Cheng, X. Zhao, W. Xue, and M. Scoble, "Using hydraulic fracturing to control caving of the hanging roof during the initial mining stages in a longwall coal mine: a case study," *Arabian Journal of Geosciences*, vol. 11, no. 20, 2018.

[20] I. Vennes, H. Mitri, D. R. Chinnasane, and M. Yao, "Large-scale destress blasting for seismicity control in hard rock mines: a case study," *International Journal of Mining Science and Technology*, vol. 30, no. 2, pp. 141–149, 2020.

[21] F. Huang, Z. Cao, S.-H. Jiang, C. Zhou, J. Huang, and Z. Guo, "Landslide susceptibility prediction based on a semi-supervised multiple-layer perceptron model," *Landslides*, vol. 17, no. 12, pp. 2919–2930, 2020.

[22] W. Tang, C. Zhai, J. Xu, Y. Sun, Y. Cong, and Y. Zheng, "The influence of borehole arrangement of soundless cracking demolition agents (SCDAs) on weakening the hard rock," *International Journal of Mining Science and Technology*, vol. 31, no. 2, pp. 197–207, 2021.

[23] X. Zhang and Y. Q. Zhang, "Experimental and numerical investigation on basic law of dense linear multihole directional hydraulic fracturing," *Geofluids*, vol. 2021, Article ID 8355737, 2021.

[24] H. Bing, R. Zhang, Y. Zeng, W. Fu, M. Yeerfulati, and M. Chen, "Analysis of hydraulic fracture initiation and propagation in deep shale formation with high horizontal stress difference," *Journal of Petroleum ence & Engineering*, vol. 170, pp. 231–243, 2018.

[25] H. B. Du, D. Feng, X. Yuan, L. Yi, and H. N. Xu, "Numerical investigation on the dynamic strength and failure behavior of rocks under hydrostatic confinement in SHPB testing," *International Journal of Rock Mechanics and Mining ences*, vol. 108, pp. 43–57, 2018.

[26] J. Huang, D. V. Griffiths, and S. W. Wong, "Initiation pressure, location and orientation of hydraulic fracture," *International Journal of Rock Mechanics & Mining Sciences*, vol. 49, no. none, pp. 59–67, 2012.

[27] Z. Liu, S. Wang, H. Ye, L. Yang, and D. Yang, "Experimental study on the effects of pre-cracks, fracturing fluid, and rock mechanical characteristics on directional hydraulic fracturing with axial pre-cracks," *Geomechanics and Geophysics for Geo-Energy and Geo-Resources*, vol. 7, no. 2, 2021.

[28] M. Souley, F. Homand, and A. Thoraval, "The effect of joint constitutive laws on the modelling of an underground excavation and comparison with _in situ_ measurements," *International Journal of Rock Mechanics & Mining Sciences.*, vol. 34, no. 1, pp. 97–115, 1997.

[29] R. Bhasin and K. Høeg, "Parametric study for a large cavern in jointed rock using a distinct element model (UDEC–BB)," *International Journal of Rock Mechanics & Mining Sciences*, vol. 35, no. 1, pp. 17–29, 1998.

[30] S. C. Blair, R. K. Thorpe, and F. E. Heuze, "Laboratory observations of the effect of geological discontinuities on hydrofracture propagation," in *Proceedings of the 30th US Symposium on Rock Mechanics*, pp. 443–450, Morgantown, West Virginia, 1989.

[31] A. A. Daneshy, "Hydraulic fracture propagation in layered formations," *Society of Petroleum Engineers Journal*, vol. 18, no. 1, pp. 33–41, 1978.

[32] H. Moon, S. Advani, and T. S. Lee, *Mathematical modeling and simulation analysis of hydraulic fracture propagation in three-layered poro-elastic media*, 1992.

[33] E. M. Llanos, R. G. Jeffrey, R. Hillis, and X. Zhang, "Hydraulic fracture propagation through an orthogonal discontinuity: a laboratory, analytical and numerical study," *Rock Mechanics and Rock Engineering*, vol. 50, no. 8, pp. 2101–2118, 2017.

[34] M. Sarmadivaleh and V. Rasouli, "Modified Reinshaw and Pollard criteria for a non-orthogonal cohesive natural interface intersected by an induced fracture," *Rock Mechanics and Rock Engineering*, vol. 47, no. 6, pp. 2107–2115, 2014.

[35] N. R. Warpinski, R. A. Schmidt, and D. A. Northrop, "In-situ stresses: the predominant influence on hydraulic fracture containment," *Journal of Petroleum Technology*, vol. 34, no. 3, pp. 653–664, 1982.

[36] J. Xie, J. Tang, R. Yong et al., "A 3-D hydraulic fracture propagation model applied for shale gas reservoirs with multiple bedding planes," *Engineering Fracture Mechanics*, vol. 228, p. 106872, 2020.

[37] Q. Zhang and X. P. Zhang, "A numerical study on cracking processes in limestone by the b-value analysis of acoustic emissions," *Computers and Geotechnics*, vol. 92, pp. 1–10, 2017.

[38] T. L. Blanton, *An Experimental Study of Interaction Between Hydraulically Induced and Pre-Existing Fractures*, Paper presented at the SPE Unconventional Gas Recovery Symposium, Pittsburgh, Pennsylvania, 1982.

[39] X. Zhang, Y. Q. Zhang, and B. X. Huang, "Investigation of the fracturing effect induced by the disturbing stress of hydrofracturing using the bonded-particle model," *Geofluids*, vol. 2021, 2021.

[40] J. Cook and J. E. Gordon, "A mechanism for the control of crack propagation in all-brittle systems," *Proceedings of the Royal Society A: Mathematical, Physical and Engineering ence*, vol. 282, no. 1391, pp. 508–520, 1964.

[41] H. Du, F. Dai, Y. Xu, Z. Yan, and M. Wei, "Mechanical responses and failure mechanism of hydrostatically pressurized rocks under combined compression-shear impacting," *International Journal of Mechanical Sciences*, vol. 165, article 105219, 2020.

[42] N. Dutler, M. Nejati, B. Valley, F. Amann, and G. Molinari, "On the link between fracture toughness, tensile strength, and fracture process zone in anisotropic rocks," *Engineering Fracture Mechanics*, vol. 201, pp. 56–79, 2018.

[43] W. Cheng, Y. Jin, and M. Chen, "Reactivation mechanism of natural fractures by hydraulic fracturing in naturally fractured shale reservoirs," *Journal of Natural Gas Science & Engineering*, vol. 23, Part 3, pp. 431–439, 2015.

[44] C. Lin, J. He, X. Li, X. Wan, and B. Zheng, "An experimental investigation into the effects of the anisotropy of shale on hydraulic fracture propagation," *Rock Mechanics and Rock Engineering.*, vol. 50, no. 3, pp. 543–554, 2017.

[45] Z. Li, L. Li, H. Bo, L. Zhang, and Q. Yu, "Numerical investigation on the propagation behavior of hydraulic fractures in

shale reservoir based on the DIP technique," *Journal of Petroleum Science and Engineering*, vol. 154, pp. 302–314, 2017.

[46] Z. Zhao, X. Li, J. He, T. Mao, G. Li, and B. Zheng, "Investigation of fracture propagation characteristics caused by hydraulic fracturing in naturally fractured continental shale," *Journal of Natural Gas Science & Engineering*, vol. 53, pp. 276–283, 2018.

[47] Y. Cheng, Y. Lu, Z. Ge, L. Cheng, and W. Zhang, "Experimental study on crack propagation control and mechanism analysis of directional hydraulic fracturing," *Fuel*, vol. 218, pp. 316–324, 2018.

[48] H. Du, F. Dai, M. Wei, A. Li, and Z. Yan, "Dynamic compression–shear response and failure criterion of rocks with hydrostatic confining pressure: an experimental investigation," *Rock Mechanics and Rock Engineering*, vol. 54, no. 2–3, pp. 1–17, 2021.

[49] X. Liu, Z. Qu, T. Guo, Y. Sun, Z. Wang, and E. Bakhshi, "Numerical simulation of non-planar fracture propagation in multi-cluster fracturing with natural fractures based on lattice methods," *Engineering Fracture Mechanics*, vol. 220, article 106625, 2019.

[50] L. Zhang, J. Zhou, A. Braun, and Z. Han, "Sensitivity analysis on the interaction between hydraulic and natural fractures based on an explicitly coupled hydro-geomechanical model in PFC2D," *Journal of Petroleum Science & Engineering*, vol. 167, pp. 638–653, 2018.

[51] J. Zhou, L. Zhang, A. Braun, and Z. Han, "Numerical modeling and investigation of fluid-driven fracture propagation in reservoirs based on a modified fluid-mechanically coupled model in two-dimensional particle flow code," *Energies*, vol. 9, no. 9, p. 699, 2016.

[52] P. A. Cundall, "A computer model for simulating progressive large-scale movements in blocky rock systems," *Proceedings of the International Symposium on Rock Mechanics*, vol. 1, no. ii-b, pp. 11–18, 1971.

[53] P. A. Cundall and O. D. L. Strack, "Discussion: a discrete numerical model for granular assemblies," *Géotechnique*, vol. 30, no. 3, pp. 331–336, 1980.

[54] X. P. Zhang and L. N. Y. Wong, "Cracking processes in rock-like material containing a single flaw under uniaxial compression: a numerical study based on parallel bonded-particle model approach," *Rock Mechanics & Rock Engineering*, vol. 45, no. 5, pp. 711–737, 2012.

[55] X. P. Zhang and L. N. Y. Wong, "Crack initiation, propagation and coalescence in rock-like material containing two flaws: a numerical study based on bonded-particle model approach," *Rock Mechanics and Rock Engineering*, vol. 46, no. 5, pp. 1001–1021, 2013.

[56] N. Cho, C. D. Martin, and D. C. Sego, "A clumped particle model for rock," *International Journal of Rock Mechanics & Mining Sciences*, vol. 44, no. 7, pp. 997–1010, 2007.

[57] Z. Jian, L. Zhang, Z. Pan, and Z. Han, "Numerical studies of interactions between hydraulic and natural fractures by smooth joint model," *Journal of Natural Gas Science & Engineering*, vol. 46, pp. 592–602, 2017.

[58] Q. Zhang and X. P. Zhang, "The crack nature analysis of primary and secondary cracks: a numerical study based on moment tensors," *Engineering Fracture Mechanics*, vol. 210, pp. 70–83, 2018.

[59] X. Zhang, Y. Q. Zhang, and T. Zhang, "Experimental and numerical investigation on hydraulic fracture propagation law of composite rock materials considering the disturbing stress effect," *Geofluids*, vol. 2021, Article ID 9920633, 2021.

[60] X. Zhang, *Hydraulic Fracture Propagation Law of Composite Rock Considering Stress Disturbance Effect*, China University of Mining and Technology, 2021, (in Chinese).

[61] E. Sharon, S. P. Gross, and J. Fineberg, "Local crack branching as a mechanism for instability in dynamic fracture," *Physical Review Letters*, vol. 74, no. 25, pp. 5096–5099, 1995.

[62] P. D. Washabaugh and W. G. Knauss, "Non-steady, periodic behavior in the dynamic fracture of PMMA," *International Journal of Fracture*, vol. 59, no. 2, pp. 189–197, 1993.